SAND98-2527J

# Stress Isotherms of Porous Thin Materials: Theoretical predictions from a nonlocal Density Functional Theory

Laura J. Douglas Frink
*Materials Simulation Science Dept.*
*Sandia National Laboratories, Albuquerque, New Mexico 87185-1111*

Frank van Swol
*Chemical Engineering Dept., Applied Materials Laboratory*
*University of New Mexico, Albuquerque, NM*
*Theoretical and Computational Materials Modeling Dept.*
*Sandia National Laboratories, Albuquerque, New Mexico 87185-1349*
(October 13, 1998)

Recent beam bending (BB) experiments of microporous films with very small pores have shown that the fluid confined in these pores exhibits monotonic compressive stresses as the relative pressure is varied from vacuum to saturation (relative vapor pressure, $p/p_o = 1$). The variation of the stress near saturation is found to be linear in $ln(p)$ and given by the saturated liquid density, $\rho_l$, to within 20%. Capillary condensed fluids are traditionally described by the Laplace-Kelvin (LK) theory. LK theory correctly predicts the slope of the stress near saturation to be $\rho_l$, but also predicts that the stress should be zero at saturation and *tensile* between saturation and the capillary transition pressure. Hence LK theory does not capture the monotonic compressive stress observed in BB experiments. This report describes the results of density functional theory calculations for a simple fluid confined to a slit pore network. We show how the presence of even a small amount of polydispersity in pore size leads to both a monotonic compressive stress as well as the observed LK slope.

## I. INTRODUCTION

Capillary condensation is of critical importance in the drying of microporous materials where pore sizes can be less than 1.0 nm. In these cases, it has been shown with both density functional theory (DFT) [1] and molecular simulation [2] that the predictions of the classical Laplace-Kelvin (LK) theory fail. In particular, the LK theory is in error regarding the pressure at which capillary condensation occurs for a pore of known size. It also fails to predict the decrease in the capillary critical temperature, $T_{cc}$, with decreasing pore size. Instead, the LK equation predicts that $T_{cc} = T_c$ (the bulk critical temperature) for all pores.

During capillary condensation, a dilute *vapor-like* pore fluid is replaced by a dense *liquid-like* fluid. This condensation produces an increase in the adsorption and an accompanying variation in pressure acting on the pore walls, $\tilde{p}$. The solvation force per unit area (or disjoining pressure) is a measure of this force and is defined as $f_s \equiv F_s/A \equiv \tilde{p} - p$ where $p$ is the pressure in the bulk solvent outside the pore.

In recent BB experiments [3], the solvation force in a microporous (pore size $< 1nm$) ceramic film formed by a sol-gel process has been measured as a function of the relative pressure of solvent in the bulk vapor phase The experiments showed a monotonically increasing solvation force with increasing relative pressure. This result directly contradicts the LK theory which predicts only *tensile* capillary stresses [4]. In addition, the magnitude of the force at saturation was many times greater than the absolute magnitude of the tensile strength of the bulk liquid. Nevertheless the slope of the force with respect to $ln\ p$ was found to be consistent with the LK theory prediction to within $\sim$ 20%! It is remarkable that the theory which fails to predict other properties in micropores is seemingly capable of correctly predicting the force variation with relative pressure.

In a previous letter both the experiments, and the results of a density functional theory (DFT) analysis were outlined. In this paper we provided a detailed description of the DFT calculations, as well as a systematic parameter study with which experiments can be compared. Specifically, in the previous communication we focused exclusively on the characterization of pore morphology, while in this paper we expand on those results and provide predictions for determining chemical properties as well as identifying expected behavior of porous networks containing both mesopores and micropores.

## II. THEORY

While the porous networks in the BB experiments are clearly complex in their geometry, we begin with a consideration of a system of uniform slit pores exposed to a simple fluid. Fluid-fluid interactions are described by the 12-6 Lennard-Jones (LJ) potential,

## DISCLAIMER

## DISCLAIMER

Portions of this document may be illegible in electronic image products. Images are produced from the best available original document.

$$u_{LJ}(r)/\epsilon = 4\left[\left(\frac{\sigma}{r}\right)^{12} - \left(\frac{\sigma}{r}\right)^{6}\right], \quad (1)$$

and pore wall - fluid interactions are given by

$$V^{ext}(z)/\epsilon = \sqrt{\frac{2}{5}}\epsilon_{wf}/\epsilon\left[\frac{1}{5}\left(\frac{\sigma}{z}\right)^{9} - \frac{3}{2}\left(\frac{\sigma}{z}\right)^{3}\right]. \quad (2)$$

where $\sigma$ is the solvent diameter, $\epsilon$ is the energy scale of fluid-fluid interactions, and $\epsilon_{wf}$ is a parameter that tunes the energy scale of fluid-pore interactions from hydrophilic to hydrophobic.

In the DFT calculations, both fluid-fluid and fluid-wall potentials are cut and shifted to zero at $r_c = 10\sigma$. In addition to solvent mediated interactions, direct wall-wall forces could be considered. However, as long as the pore sizes are nearly static as is the case in the BB experiments [3], the wall-wall forces will not vary with relative pressure, and hence will not vary through the course of an experiment. We therefore set the wall-wall forces to zero through the remainder of this discussion.

The solvation force in slit-like pores of size $h$ is defined as the derivative of the surface free energy with respect to the pore size [5],

$$f_s = -\left(\frac{\partial \Omega_s/A}{\partial h}\right)_{\mu,T}, \quad (3)$$

where $\Omega_s/A = \Omega/A + ph$, and $\Omega/A$, the grand free energy per unit area, is

$$\begin{aligned}\Omega[\rho(1)] = \quad & kT\int d1\ \rho\left\{\ln\left[\Lambda^3\rho(1)\right] - 1\right\} \\ & + \int d1\ \Phi\{\bar{\rho}_\gamma(1)\} \\ & + \int d1 \int d2\ \rho(1)\rho(2)u_{LJ}^{att}(1,2) \\ & + \int d1\ \rho(1)[V^{ext}(1) - \mu]. \end{aligned} \quad (4)$$

The first term in Eq. 4 is an ideal gas contribution, the second term is an excess free energy describing the volume exclusion of the fluid particles at short range, the third term is an excess free energy treating the attractions in the fluid in a strict mean field approximation, and the last term includes the external field and the solvent chemical potential, $\mu$. The attractive part of the potential energy is given by the WCA [6] split where $u_{LJ}^{att}(r) = u_{LJ}(r_{min})$ for $r \le r_{min}$ and $u_{LJ}^{att}(r) = u_{LJ}(r)$ otherwise. The volume exclusion term consists of a hard-sphere free energy density, $\Phi$, which is a function of the weighted densities, $\bar{\rho}_\gamma, \gamma = 1 - 4$). The expression for $\Phi$ was derived by Rosenfeld [7], and comes from scaled particle theory, which also provides the inspiration for the weight functions used.

The DFT is performed to numerically minimize this functional with respect to variations in the density profile between the plates via

$$\frac{\delta\Omega}{\delta\rho(1)} = 0. \quad (5)$$

In all that follows, we restrict ourselves to one temperature close to the triple point, namely $kT/\epsilon = 0.74$. For the Lennard-Jones fluid with hard-core repulsions and a strict mean field treatment of the attractions, the saturation pressure $p_o$ and densities, $\rho_l$ and $\rho_v$ at $kT/\epsilon = 0.74$ using the Percus-Yevick equation of state are:

$$\begin{aligned}\beta p_o\sigma^3 &= 0.001938 \\ \rho_v\sigma^3 &= 0.001972 \\ \rho_l\sigma^3 &= 0.8228 \end{aligned} \quad (6)$$

where $\beta = 1/kT$ and $k$ denotes Boltzmann's constant.

## III. MONODISPERSE PORES

In LK thoery, it is assumed that the capillary condensed fluid as a spatially **uniform** liquid-like density in the pore. Within this assumption, the solvation force per unit area is $f_s = p_l^\dagger - p$ where $p$ is the bulk pressure in the surrounding vapor, and $p_l^\dagger = p - 2\gamma_{lv}cos\theta/h_t$ is the pressure of a *metastable* bulk liquid at the same chemical potential as the fluid confined inside the pores. The metastable liquid pressure depends on the surface tension of the liquid-vapor interface, $\gamma_{lv}$, the contact angle, $\theta$, and the size of the pore where the capillary transition occurs at a known relative pressure, $h_t$. The solvation force is then

$$f_s(\mu,T)/A = \begin{cases} 0 & ;h > h_t \\ -2\gamma_{lv}(T)\cos\theta(T)/h_t(T,\mu) & ;h \le h_t \end{cases} \quad (7)$$

Assuming the vapor is an ideal gas and that $cos\theta = 1$ (for a "hydrophilic" or completely wetting surface), we obtain

$$f_s(\mu,T)/A \approx \begin{cases} 0 & ;h > h_t \\ kT\rho_l ln(p/p_o) & ;h \le h_t \end{cases} \quad (8)$$

where $\rho_l$ is the density of the bulk liquid at coexistence. Taking the derivative of the solvation force with respect to $ln\ p$ yields the simple result

$$\left(\frac{\partial f_s}{\partial lnp}\right)_T = \begin{cases} 0 & ;h > h_t \\ kT\rho_l & ;h \le h_t \end{cases} \quad (9)$$

Equations 8 and 9 imply two simple tests that can be performed with DFT. The first is to find the limiting value of the solvation force when $p \to p_o$. This force is predicted to be zero by the LK theory. The second test is to find the slope of the $f_s$ vs. $ln\ p$ curve at $p/p_o = 1$ which is predicted to be equal to $kT\rho_l$.

In Fig.1A, the solvation force calculated with DFT is plotted as a function of the pore size, $h$, at $p/p_o \approx 1$. In

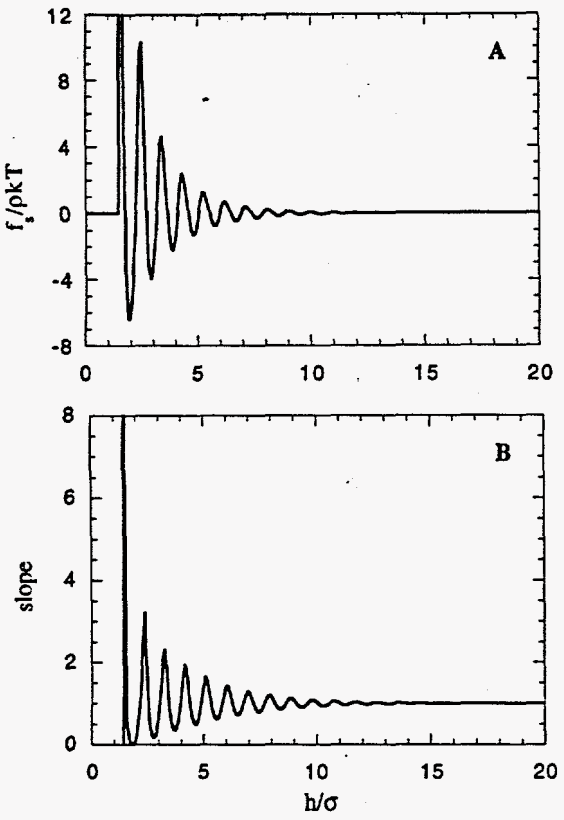


FIG. 1. (A) The solvation force, $f_s/\rho_l kT$ and (B) the numerical derivative of the solvation force $slope = \partial(f_s/\rho kT)/\partial ln\ p$ as a function of pore size for a Lennard-Jones fluid near saturation in a slit pore where $kT/\epsilon = 0.74$ and $\rho_b\sigma^3 = 0.001972$. The normalizing liquid density is $\rho_l\sigma^3 = 0.807$.

contrast to LK theory, the DFT calculations show that the solvation force is **not** a constant for all pore sizes smaller than some $h_t$. Rather, the solvation force is oscillatory, reflecting the packing constraints that will at times produce attractions and at other times produce repulsions on the pore walls. These oscillatory forces are consistent with other microscopic measures of surface forces, most notably surface forces measurements [9].

Fig. 1B shows the slope of the force with respect to the natural log of the relative pressure. As with the force, the slope oscillates about the LK value, and we obtain the LK prediction for large pores $h/\sigma > 15$ Again, the oscillations in the slope reflect the packing constraints of confined fluid.

Consequently, there are many *discrete* candidate pore sizes roughly $1\sigma$ apart for which the slope at saturation predicted by LK theory will be perfectly satisfied, but in general one must expect very large deviations for a single micropore. Thus we conclude that the framework provided by DFT for a of monodisperse porous network is not sufficient to explain beam bending experiments. This leads us to consider the role of polydispersity.

## IV. POLYDISPERSE PORE NETWORKS

While, the DFT predictions for monodisperse pores are not consistent with BB results, the fact that both the solvation force and its slope oscillate about the LK theory limits suggests that even a relatively narrow pore size distribution might lead to a slope that is close to the LK prediction.

To test the effects of polydispersity we assume a (truncated) Gaussian pore size distribution and vary the mean pore size, $h$, and the standard deviation, $t$. To be specific, we assume a pore size distribution given by:

$$\mathcal{P}(h';h) = \begin{cases} Be^{-(h'-h)^2/2t^2} & ;|h'-h| \le 2t \\ 0 & ;otherwise \end{cases} \qquad (10)$$

Where $B$ is a normalization constant. A particular average property $< X >$ of an *ensemble* of pores is then easily expressed in terms of the property $X(h')$ of a particular pore of size $h'$, and its probability, $\mathcal{P}(h';h)$. Thus,

$$< X > (h) = \int_0^\infty dh' X(h')\mathcal{P}(h';h). \qquad (11)$$

The effects of polydispersity on the solvation force and its limiting slope are shown in Fig. 2 for the cases $t/\sigma = 0, 0.2, 0.3$, and $0.5$. The introduction of polydispersity reduces the amplitude of oscillations in both the force and its slope. However, while the slope averages to the LK limit for almost all cases ($\bar{h}/\sigma \ge 1.6$ and $t/\sigma \ge 0.3$), the force remains positive for small pores ($\bar{h}/\sigma \le 4$ and $t/\sigma \ge 0.3$) in conflict with the LK prediction of zero stress at saturation.

The residual compressive force found for the polydisperse pore model is due to an inherent asymmetry in the oscillatory force curve. This assymetry arises from the low compressibility of a single layer of fluid confined in a pore. As was noted in the introduction, both the LK slope and the compressive stress at saturation have been observed in BB experiments. Thus, we can immediately conclude that *both* a small degree of polydispersity ($t/\sigma \approx 0.3 - 1.0$) in pore size *and* a small mean pore size ($\bar{h}/\sigma \le 4$) are necessary to reproduce the results of the BB experiments at saturation. Conversely, in order to measure the force oscillations of the previous section, a single well defined pore (such as the SFA) or a nearly monodisperse system of pores is required.

## V. CHARACTERIZING PORE PROPERTIES FROM STRESS ISOTHERMS

In BB experiments, stress isotherms (solvation force as a function of relative pressure) are obtained. Therefore, we have calculated solvation forces for a wide range of mean pore sizes, $\bar{h}/\sigma$, widths of pore size distribution, $t/\sigma$, sorbate relative pressures, $p/p_o$, and solvent-surface

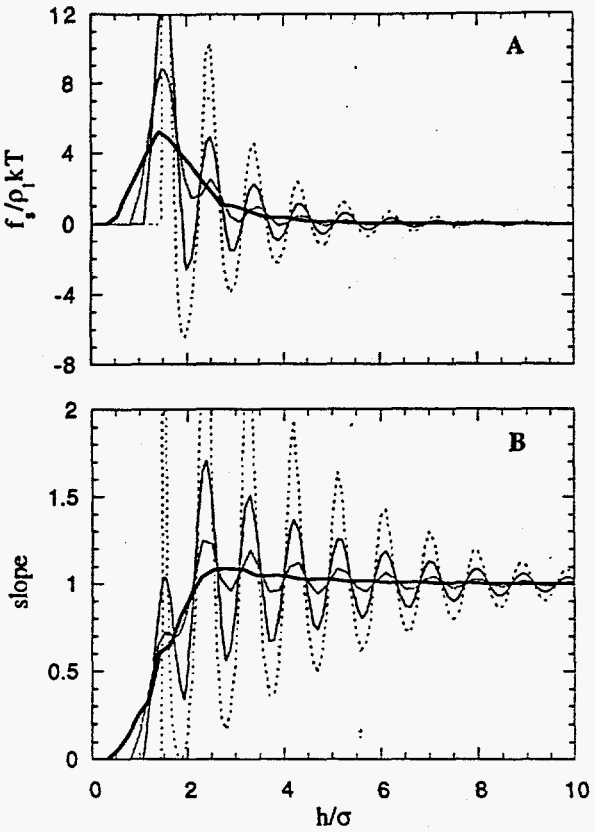


FIG. 2. (A) The mean solvation force $f_s = \bar{f}_s$ and (B) the numerical derivative of the mean solvation force, $slope = \partial \bar{f}_s/\rho kT/\partial ln\ p/p_o$ as a function of mean pore size, $h = \bar{h}$, for fluids confined in microporous polydisperse pore networks. The dashed line corresponds to monodisperse pores while the solid curves show the polydisperse network results. In order of decreasing amplitude the solid curves correspond to $t/\sigma = 0.2, 0.3$, and 0.5.

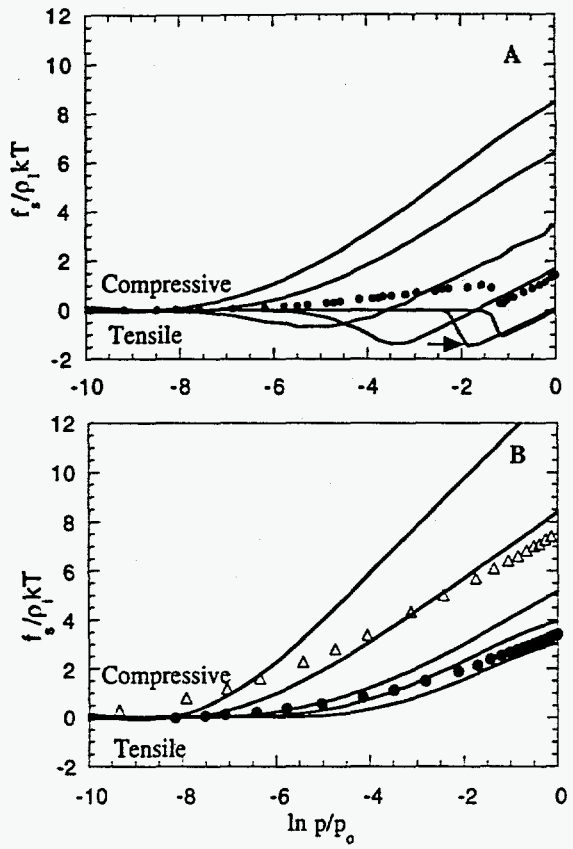


FIG. 3. The mean solvation force, $f_s = \bar{f}_s$ as a function of the log of the relative pressure for a fluid confined in polydisperse networks of slit-like pores characterized by (A) $t/\sigma = 0.3$ and (B) $\bar{h}/\sigma = 1.6$. All curves represent best fits through the DFT data; for examples of the expected scatter see Fig.6. The various solid curves in A are distinguished by different mean pore sizes. From top to bottom at saturation, they are: $\bar{h}/\sigma = 1.60$, $\bar{h}/\sigma = 1.74$, $\bar{h}/\sigma = 1.90$, $\bar{h}/\sigma = 2.70$, $\bar{h}/\sigma = 4.72$ (indicated with arrow), and $\bar{h}/\sigma = 6.72$. The dotted line in A is a stress isotherm for a bimodal distribution of pores composed of 20% small pores centered on $\bar{h}/\sigma = 1.74$ with $t/\sigma = 0.3$ and 80% larger pores centered on $\bar{h}/\sigma = 6.72$ with $t/\sigma = 0.3$. The solid curves in B are distinguished by different gaussian distribution half-widths. From top to bottom they are: $t/\sigma = 0.2, 0.3, 0.5, 0.7$, and 1.0. The symbols in B are experimental results for (•) t-butanol in a P-25 film and (△) methanol in an A2 film [3].

interactions, $\epsilon_{wf}$. The DFT predictions may be compared with BB isotherms to predict $\bar{h}$, $t$, and $\epsilon_{wf}$ for a given film and sorbate. In this section, we detail how this characterization may be accomplished.

### A. Pore Size

Fig.3A shows DFT stress isotherms for pore networks where the mean pore size ranges from $\bar{h}/\sigma = 1.6$ to $\bar{h}/\sigma = 6.72$ while the half width of the gaussian distribution is fixed at $t/\sigma = 0.3$. Fig.3B shows stress isotherms for a mean pore size of $\bar{h}/\sigma = 1.6$, and $t$ ranging from $t/\sigma = 0.2 - 1.0$. In both cases, $\epsilon_{wf} = 5.0$ which is found in the complete wetting ($cos\theta = 1$) regime.

In all of the isotherms in Fig.3, the LK slope is recovered (within 20%) in the limit $p/p_0 \to 1$. However monotonic compressive stresses are only found for the smallest pores, $\bar{h}/\sigma = 1.6$ and 1.74 in Fig.3A. Density profiles show that only one layer of fluid particles is adsorbed in pores of these sizes.

In contrast, the pores that are large enough for four or more layers of atoms ($\bar{h}/\sigma = 4.72$ and 6.72 in Fig.3A) display LK tensile behavior for $p_t < p < p_o$. In addition, these large pores return to the LK limit of $f_s \rightarrow 0$ as $p \rightarrow p_o$. The intermediate pore sizes where two adsorbed layers may be present in the pore, $\bar{h}/\sigma = 1.90$ and 2.70 display both compressive (at high relative pressures) and tensile (at lower relative presures) behavior.

The DFT results for the largest pores demonstrate that the correct limiting LK behavior is exhibited by the DFT. The results for the smallest pores indicate that severe constraints are placed on the mean pore size of an unknown film in order for that film to exhibit a monotonic compressive stress isotherm. Specifically, a monotonic compressive isotherm must have $1.55 \leq \bar{h}/\sigma \leq 1.75$. Thus it is possible from the *qualitative* features of the stress isotherm to establish pore size to within $\pm 0.1\sigma$ for micropores [8]. Contrast this to adsorption isotherms where the qualitative features of the isotherm do not vary enough for small pores to make this distinction.

### B. Bimodal Distributions

In BB experiments on a variety of films and sorbate molecules, all three of the predicted qualitative behaviors shown in Fig.3A (monotonic compressive, tensile, and mixed) have been observed [3,10]. In addition, in films that were specifically fabricated to produce bimodal distributions, showed a compressive stress isotherm with a dip below saturation [10].

A stress isotherm corresponding to a simple model bimodal distribution is shown in the dotted line of Fig.3A. This curve has a pore size distribution that is a summation of 20% small pores ($\bar{h}/\sigma = 1.74$) and 80% larger pores ($\bar{h}/\sigma = 6.72$). This result from DFT calculations shows a dip that is similar to those found in the experiments.

The dip in the stress shown in the dotted line in Fig.3 is a hallmark of a bimodal pore size distribution. When such an isotherm is obtain, several conclusions can be reached. First the distribution must contain micropores because the compressive stress at saturation can only be attributed to these small pores. The larger LK pores have no contribution at saturation. In addition, the bottom of the dip in the isotherm occurs at the capillary transition point of the large pores. An approximate pore size for the larger (mesoscopic) can be calculated based on the location of the capillary transition pressure from LK theory. Finally, if the saturation value of the stress isotherm for a purely small pore material can be estimated or measured, the fraction of large and small pores can be estimated.

### C. Width of Distribution

In Fig.3B the width of the pore size distribution is varied, but $\bar{h}$ is held constant at $\bar{h} = 1.6\sigma$ where all of the isotherms are monotonic and compressive. In all cases, $t/\sigma \leq 1$, so these distributions are very narrow (a few Angstroms) in an absolute sense. As the pore size distribution becomes wider, the magnitude of the stress decreases. For comparison, two experimental stress isotherms are included in Fig.3B.

While the mean pore size in the microscopic regime can be accurately established on the basis of the qualitative features of the isotherm, the accuracy of $t/\sigma$ estimates depends on the actual stresses measured. There are several ways in which experiments could be compared with DFT calculations to establish $t$; we have chosen to compare the value of the stress at saturation.

Fig.4 shows the variation of the solvation force at saturation with $t/\sigma$ for various pore sizes ($\bar{h}/\sigma = 1.5 - 1.75$). Over the range $0.2 \leq t/\sigma \leq 1.0$, the saturation stress changes by a factor of approximately 3. This rapid variation of saturation stress with $t$ allows an estimation of $t$ to within $\pm 0.02\sigma$ if $\bar{h}$ is known.

If both $\bar{h}$ and $t$ are unknown (as will most often be the case), the errors in estimating $t$ will depend on its value. Fig.4 shows that when $t/\sigma > 0.5$, the stress response is insensitive to $\bar{h}/\sigma$. In this regime the high degree of accuracy is therefore expected for an estimation of $t$. On the other hand, when $t/\sigma < 0.5$, the stress response for different pore sizes begin to diverge. Thus, the errors in estimating $h$ will result in larger errors when estimating $t$.

One way to achieve accurate estimates of $t$ even for the narrower pore size distributions, is to expose a given film to a variety of adsorbates that differ in size. As the size of the probe molecule ($\sigma$) decreases, the ratios $t/\sigma$ and $h/\sigma$ increase since $t$ and $h$ are fixed material properties. It therefore may be possible to push $t/\sigma$ to the most accurate regime by decreasing sorbate size. In our previous letter [3], one film (designated P-25) was exposed to a series of alcohols in an effort to determine $t/\sigma$, and to establish the effect of varying $t/\sigma$ on the stress isotherms. As DFT predicts (see Fig.3B), the experiments showed decreasing stress with decreasing sorbate size (increasing $t/\sigma$).

### D. Chemical Interactions

In addition to pore morphology, it is possible to characterize in a global sense the pore-fluid chemistry. In the model, the pore-fluid chemistry is related only to the surface fluid interaction parameter, $\epsilon_{wf}$. As this parameter varies the contact angle, $\theta$ may vary from 180° (complete drying or hydrophobic) to 0° (complete wetting or hydrophilic) [2]. Fig.5 shows the variation of $cos\theta$ with $\epsilon_{wf}$.

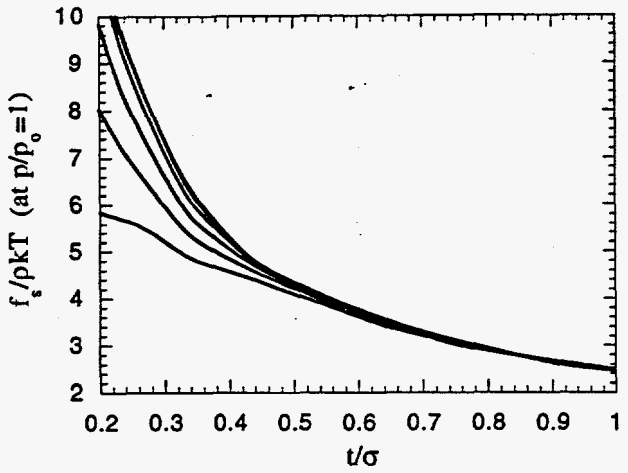


FIG. 4. The average solvation force, $f_s = \bar{f}_s$ at saturation ($p/p_o = 1$) as a function of the width of the pore size distribution, $t/\sigma$. The various curves have different mean pore sizes. From top to bottom, they are: $\bar{h}/\sigma = 1.5$, $\bar{h}/\sigma = 1.55$, $\bar{h}/\sigma = 1.6$, $\bar{h}/\sigma = 1.65$, $\bar{h}/\sigma = 1.7$, $\bar{h}/\sigma = 1.75$. Note that $\bar{h}/\sigma = 1.5$ and 1.55 curves are nearly indistinguishable.

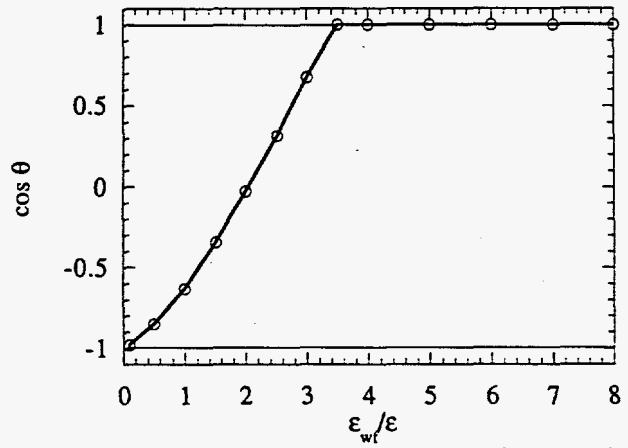


FIG. 5. The cosine of the contact angle as a function of the wall-fluid interaction potential parameter, $\epsilon_{wf}$.

In Fig.6 the variation of the stress isotherms with changes in $\epsilon_{wf}$ is shown. As $\epsilon_{wf}$ decreases, the magnitude of the stress decreases, and the relative pressure at which a nonzero stress is first measured (the take-off point) shifts to higher relative pressure. The shift in the take-off point is striking as it varies from $-16 \leq lnp/p_o \leq -2$. In contrast, for all $t/\sigma$ and $\bar{h}/\sigma$ in Fig.3 (except the cases $\bar{h}/\sigma > 4$) the take off point is found in the range $-8 \leq lnp/p_o \leq -6$. The lack of variation in take-off point in previous calculations suggests that the take-off point is more sensitive to $\epsilon_{wf}$ than to either $\bar{h}$ or $t$. To first order, the strength of wall-fluid interactions may be estimated from the take-off point alone.

For the two experimental results shown in Fig.3B, the take-off points appear to be located at $lnp/p_o \approx -10$ (A2) and $lnp/p_o \approx -8$ (P-25). These observations suggest that the A2/methanol interaction is stronger than the P-25/t-butanol interaction. For improved accuracy

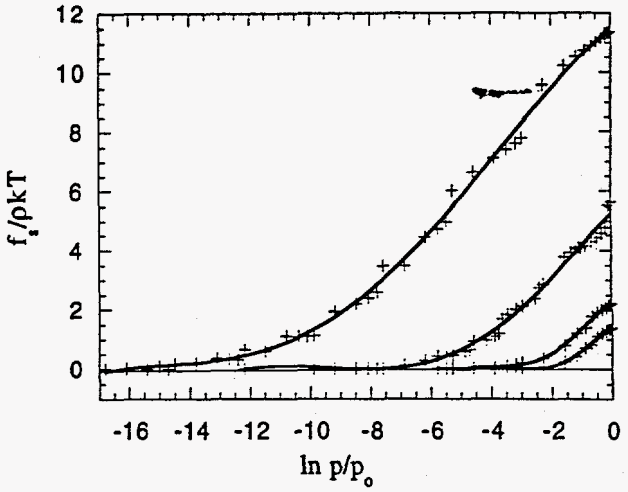


FIG. 6. (A) The average solvation force, $f_s = \bar{f}_s$ as a function of relative saturation for polydisperse networks of pores where $\bar{h}/\sigma = 1.6$ and $t/\sigma = 0.5$. The various curves are distinguished by different values of the wall-fluid interaction parameter, $\epsilon_{wf}$. From top to bottom, the curves have: $\epsilon_{wf}/\epsilon = 8$, $\epsilon_{wf}/\epsilon = 5$, $\epsilon_{wf}/\epsilon = 3.5$, and $\epsilon_{wf}/\epsilon = 3.0$. The (+) symbols indicate actual DFT data points, the lines are best smooth fits to the data.

in predicting $\bar{h}$ and $t$, slightly different values of $\epsilon_{wf}/\epsilon$ should be used for each film. The particular $\epsilon_{wf}$ would be chosen to match the experimentally observed take-off point. For experimental data presented here, the take-off points were sufficiently close that substantial errors do not result from assuming both systems have $\epsilon_{wf}/\epsilon = 5$.

One significant difference in DFT and LK predictions can be found in the limit $cos\theta \to 1$. Fig.6 correctly shows that the stress response does not saturate when $cos\theta = 1$ as LK theory would predict. As a result, if the stress isotherms for two fluids which are both perfectly wetting on a given material are compared, it is possible to determine in which case the surface-fluid interactions are stronger using the DFT analysis presented here.

## VI. CONCLUSIONS

In this paper, we have demonstrated that stress isotherms measured with a beam bending experiment can be interpreted with a molecular theory that captures solvent packing effects in confined geometries. The DFT captures all the relevant qualitative aspects of the experimental data including monotonic compressive stresses and the LK slope at saturation.

At the quantitative level, the DFT results can be used to predict the mean pore size, degree of pore size polydispersity, and sorbate-surface interactions. The BB experiment along with the DFT interpretation provided here is therefore a new method for the characterization of microporous thin film materials.

The quality of the DFT characterization is surprising considering the simple model pore network we have considered (slit-like pore networks). We can only conclude that the geometry of the pore is secondary in importance to (1) the existence of polydispersity and (2) the strong adsorption of a single fluid layer in the micropores. This strong adsorption ultimately gives rise the the very large first compressive peak in the solvation force curve of a single pore (see Fig.1A), and it is this large peak which leads to the observed compressive stresses. The fact that the last layer of fluid will be most strongly adsorbed and therefore will always lead to large solvation forces is to be expected independent of the pore geometry considered.

At a more fundamental level, the observation of a nonzero stress at saturation in these microporous materials proves the existence of nonzero short range solvation forces in complex porous media. In addition, and perhaps most importantly, the BB experiment is a new device for measuring short-range solvation forces.

Determining solvation forces is an important issue that affects many areas of science, but there are anxiously few probes available. At present there are three techniques for measuring short-range solvation forces : the surface forces apparatus [9], the atomic force microscope, and the osmotic stress device [11,12]. Of these the first two both measure force and surface separation directly for a single well defined pore. The osmotic stress device may be used to determine the surface-surface interaction more indirectly through a measurement of the osmotic pressure of a collection of suspended objects (e.g. colloidal particles, membranes) [11]. The surface separations are measured directly in the osmotic stress device by means of X-ray scattering.

In contrast, the beam bending device provides a direct measurement of the mean force in a complex porous material. While osmotic stress and beam bending techniques may be arguably less elegant than the truly microscopic alternatives provided by the SFA and AFM, the OSD and BB experiments are also far more powerful in probing the solvation forces acting between complex materials in their natural environments.

In this paper we have studied the response of the solvation force to variations in both molecular parameters and pore morphologies The picture provided here is completely consistent with SFA measurements in that the results ultimately stem from force oscillations due to packing constraints in single pores. Thus this paper provides the theoretical groundwork that links these two experiments.

## ACKNOWLEDGMENTS

The authors would like to thank J. Samuel and C.J. Brinker for their insightful experiments and stimulating discussions.

This work was performed at Sandia National Laboratories. Sandia is a multiprogram laboratory operated by Sandia Corporation, a Lockheed Martin Company, for the United States Department of Energy under Contract DE-AC04-94AL85000.

---

[1] Evans, R. and Marini Bettolo Marconi, U., J. Chem. Phys., **1987**, *86*, 7138.

[2] van Swol, F. and Henderson, J.R., Phys. Rev. A, **1989**, *40*, 2567. Phys. Rev. A, **1991**, *43*, 2932.

[3] Samuel, J.S., Brinker, C.J., Douglas Frink, L.J., and van Swol, F., Langmuir, **1998**, *14*, 2602.

[4] Rowlinson, J.S. and Widom, B., *Molecular Theory of Capillarity*, (Oxford Univ. Press, Oxford), 1982.

[5] Henderson, J.R., Mol. Phys., **1986**, *59*, 89.

[6] J.D. Weeks, D. Chandler, and H.C. Anderson, J. Chem. Phys., **1971**, *54*, 5237.

[7] Rosenfeld, Y., Phys. Rev. Lett., **1989**, *63*, 980.

[8] Note that in [3] when identifying pore sizes, we defined a pore to be the *size of the solvent molecule* if the density profile has one peak, the solvation force is zero (it is an unstressed state), and the slope of the solvation force is negative (it is a thermodynamically stable state). These conditions are met not at $h/\sigma = 1.0$, but rather at $h/\sigma \approx 1.75$ (see Fig.1).

[9] R.G. and Israelachvili, J.N., J. Chem. Phys., **1981**, *75*, 1400.

[10] communication with J.Samuel and C.J. Brinker

[11] Rau, D.C. and Parsegian, V.A., Biophys. J., **1992**, *61*, 260.

[12] Frink, L.J.D. and F. van Swol, J. Chem. Phys., **1994**, *100*, 9106.